MARS' SOUTHERN HEMISPHERE: INFLUENCES OF THE GREAT IMPACT BASINS ON EXTRATROPICAL WEATHER AND THE WATER CYCLE. Jeffery L. Hollingsworth[1], Melinda A. Kahre[1], Robert M. Haberle[1], [1]Space Science and Astrobiology Division, Planetary Systems Branch, NASA Ames Research Center, Moffett Field, CA 94035, (jeffery.l.hollingsworth@nasa.gov).

Introduction: Large-scale, extratropical weather disturbances (i.e., high- and low-pressure systems or "transient synoptic-period baroclinic/barotropic waves") are critical components of the global (i.e., general) circulation of a rapidly rotating, differentially heated, shallow atmosphere such as on Earth and Mars. Critically, these wave-like disturbances act as agents for the transport of heat and momentum between low and high latitudes of the planet, and co-incidingly, for the transport of tracers within the atmosphere (e.g., aerosols such as water vapor/ice and dust for Mars).

Measurements provided by the Mars Global Surveyor (MGS) thermal emission spectrometer (TES) instrument and the Radio Science (RS) occultation investigation have provided, for the first time, unequivocal evidence that the middle and high latitudes of Mars' southern hemisphere (SH) experiences large-scale, traveling weather systems [1–3]. Prior to these atmospheric measurements and traveling-wave analyses, a variety of atmospheric circulation model investigations [4–6] postulated that such large-scale extratropical disturbances ought to be present in this hemisphere. In addition, over a similar seasonal span (e.g., NH late autumn/SH late autumn; NH winter/SH winter; etc), such theoretical and atmospheric modeling studies, and the MGS/TES and RS observations, have indicated that the vigor of the SH transient waves is much less intense and the depth scales shallower, compared to their northern hemisphere (NH) counterparts. Although temperature amplitudes can be $\mathcal{O}$(2–10$\times$) weaker, mostly similar wave mode scales (wavenumbers 1-3) and periods (e.g., 2–4 days at low levels; 6–20+ days at upper levels) are found for the southern extratropical waves.

In some ways similar to the northern hemisphere, during late autumn and winter, the southern extratropics exhibits a dominant "storm track" (or "storm zone"), where the intensity of, and associated atmospheric variability with, the traveling weather disturbances is the most intense and regionalized geographically. At low atmospheric levels in the SH extratropics (e.g., below a 1-2 scale heights), the variability is greatest in the western hemisphere, roughly between the Tharsis highlands and the prime meridian [1–3]. The SH storm zone appears more intense during SH late winter and early spring [1–3].

Fundamental to assessing the present climate of Mars is forming an understanding of its water cycle via spacecraft observations, theoretical studies and modeling. Recent spacecraft missions (e.g., Mars Express (MEX), Mars Reconnaissance Orbiter (MRO)) have provided new measurements critical to key components of this cycle, in particular, both seasonal and interannual variations in atmospheric water column abundance, water ice cloud occurrence and surface ice/frost distribution [1–6]. Global climate models of Mars have been used to investigate key atmospheric and surface aspects of Mars' water cycle [7] and more recently, the nature of cloud microphysical processes [8,9]. Such modeling tools, combined with the recent observations, serve to illuminate underlying meteorological processes that give rise to water vapor transport, water-ice cloud formation and their spatial and temporal variabilities, and the interactions of atmospheric circulation components (e.g., mean overturning cells, small- and large-scale waves, etc) with them. Here we make use of recent high-resolution observations of the seasonal southern polar cap, together with a general circulation model, to assess large-scale structures in near-surface and within the atmosphere water vapor condensation/sublimation and surface ice deposition.

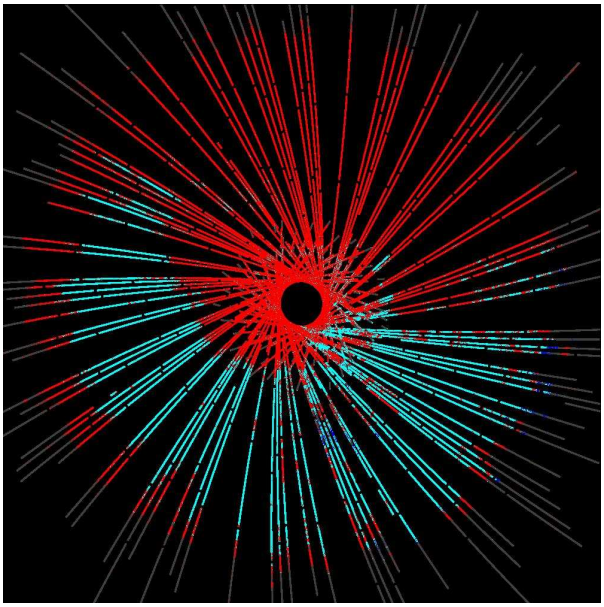

Fig. 1: South polar stereographic projection (latitudes $> 55°$S) of CRISM multispectral (MSP) observations obtained during early spring ($L_s = 183.5 - 191.0°$) of CO_2 and H_2O near-surface during MY 28 (February through July 2007): pure CO_2 ice (red); pure H_2O ice (dark blue); mix of CO_2/H_2O ice (cyan); no ice (gray). (Courtesy Adrian Brown, SETI Institute)

Observations: Recent measurements obtained by the Compact Reconnaissance Imaging Spectrometer for Mars (CRISM) instrument onboard MRO have been projected into polar stereographic maps to investigate the

retreat of the southern seasonal polar ice cap, and the distribution of both CO_2 and H_2O ice [16]. The CRISM multispectral (MSP) strips from MRO's primary mission have a nominal resolution of 185m/pixel [17] and consist of long channel (1.0-4.0 μm) measurements. A sample south polar mosaic during early spring ($L_s \sim 187.3°$) compiled over fourteen days of CRISM MSP strips is shown in Fig. 1. The coloring of the strips in the mosaic corresponds to the following: CO_2 ice (red); pure H_2O ice (dark blue); mixture of CO_2/H_2O ice (cyan); and, no ice (gray). It can be seen from Fig. 1 that significant east-west (longitudinal) asymmetries occur in the southern extratropics and high latitudes with respect to the type of near-surface condensate (i.e., CO_2 ice, H_2O ice or a mixture of the two). From the measurements utilized to created the polar mosaics thus far, it is not possible to discriminate between low-level water-ice clouds or surface deposits (a work in progress).

To explore the nature of such longitudinal asymmetries we have utilized a recent version of the NASA Ames Mars general circulation model (MGCM) which simulates the seasonal and spatial variations in the Mars water cycle with reasonable fidelity.

Climate Model: We have utilized the NASA Ames MGCM version 2.1 to simulate the present water cycle on Mars [12]. This version runs with an updated radiation code (based on a two-stream approximation with correlated k's), and a cloud microphysics scheme that assumes a log-normal particle size distribution whose first two moments are carried as tracers, and which includes the nucleation, growth and sedimentation of ice crystals [9]. In addition, atmospheric dust is partially interactive in this simulation. The radiation code actually responds to a prescribed distribution based on an opacity climatology derived from MGS Thermal Emission Spectrometer (TES) 9-μm opacity measurements during the first mapping year, and the vertical distribution varies with season and latitude [9]. The cloud microphysics code interacts with a transported dust tracer whose surface source is adjusted to maintain an atmospheric column abundance as observed by TES. In our initial simulations, water-ice clouds are radiatively passive. Our model configuration is G30L24 which corresponds to a horizontal resolution of $5 \times 6°$ latitude-longitude, with 24 unequally-spaced vertical layers that have higher vertical resolution near the surface. The model top is placed at approximately 80 km. For initialization, the simulation is started from an isothermal, circulation-free and dry atmosphere, with the only source for water vapor specified in terms of a uniform polar north residual cap (NRC) that extends poleward from $80°$N. The simulation is run to a water-cycle equilibrium which is achieved within five Mars years.

Results and Diagnostics: We have analyzed both time-mean and eddy (i.e., stationary and synoptic-period transient) structures in our Mars GCM simulations. Here, time means centered on a given season (L_s) are constructed using 30 days of simulation, and transient meteorological fields have been band-pass filtered such that variability only associated with synoptic-period wave disturbances is captured.

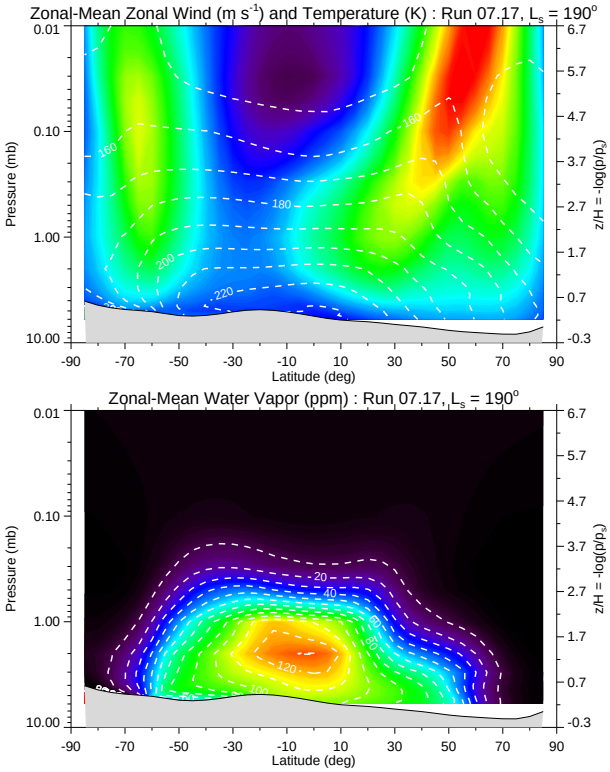

Fig. 2: The time and zonally averaged (a) temperature (K) and zonal wind (m s^{-1}) and (b) water vapor mixing ratio (ppm) during early southern spring (L_s = 190°) from the Mars GCM simulation. The contour interval is 10 K and 10 ppm in (a) and (b), respectively.

During early southern spring (L_s = 184°), the time and zonally-averaged field of water vapor exhibits a pattern resembling the mean thermal structure, that is, one nearly symmetric about the equator. This near-equatorial symmetric structure can be clearly seen in Fig. 2. Water-ice cloud distributions, however, are not as equatorially symmetric: there is an enhancement of clouds in the tropics aloft (0.5 mbar) and high southern latitudes at low levels of the atmosphere.

Further inspection of the spatial distribution of water vapor and water-ice clouds in a longitudinal sense indicate significant asymmetries in such fields between eastern and western hemispheres of the southern extratropics. These east-west asymmetries are depicted in Fig. 3. The top panel of this figure shows the time-mean mixing ratio of water vapor at 3.5 mbar. The middle panel depicts the so-called "stationary" pattern of the same field (i.e., the longitudinal means have been removed). The east-west asymmetries are more easily seen in this panel, where the bulk of the western hemisphere appears drier than that of the eastern hemisphere.

There is a significant enhancement of low-level water vapor in the western hemisphere and a depleted concentration in the eastern hemisphere. This distribution of the water vapor field is likely associated with large-scale quasi-stationary (i.e., Rossby) waves and their associated circulation components and water vapor fluxes. In addition, water-ice clouds appear to form preferentially in the western hemisphere at low-levels and are nearly absent in the eastern hemisphere. At higher altitudes (0.1 mbar) there is considerable enhancement, however, in ice-cloud activity in longitudes bracketing the Hellas corridor. The bottom panel of Fig. 3 shows day-to-day variability in the water vapor field associated with transient waves (i.e., synoptic period weather disturbances). There is a geographic preference in this variability between the southern extent of the Tharsis higlands and the Hellas impact basin. As noted above, this is the same location of the SH storm zone as seen in MGS/TES and RS data.

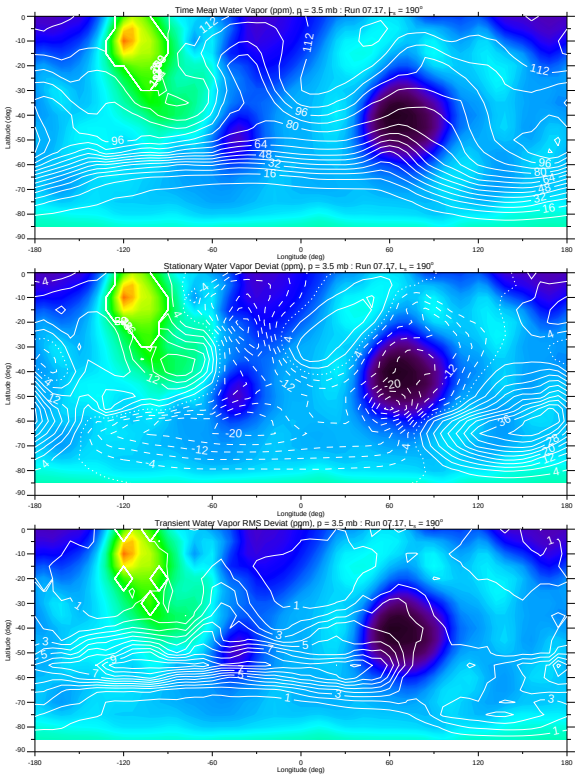

Fig. 3: The (a) time mean water vapor (ppm), (b) stationary water vapor (ppm) and (c) transient water vapor (ppm) at 3.5 mbar during early southern spring (L_s = 190°) from the Mars GCM simulation. The contour interval is 8, 4 and 1 ppm, in panels (a)–(c), respectively.

Potential wave-induced impacts from SH transient-eddy variability on the mean atmospheric state has been examined using a localized wave activity flux (i.e., a 3D (transient) generalization of the Eliassen-Palm flux), as developed by *Hoskins et al.* [20] and *Trenberth* [21]. The Hoskins/Trenberth flux, E_u, is given by

$$E_u = (E_u^{(\lambda)}, E_u^{(\varphi)}, E_u^{(z)}) \quad \& \quad \overline{u}_t \propto \frac{\nabla \cdot E_u}{\cos\varphi}$$

where

$$\begin{aligned} E_u^{(\lambda)} &\equiv 1/2(\overline{v'^2} - \overline{u'^2})\cos\varphi \\ E_u^{(\varphi)} &\equiv -\overline{u'v'}\cos\varphi \\ E_u^{(z)} &\equiv (fRH^{-1}N^{-2}\overline{v'T'} - \overline{u'w'})\cos\varphi \end{aligned}$$

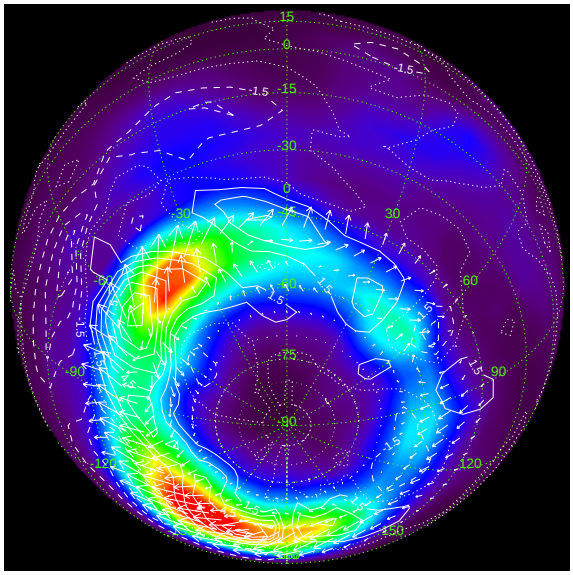

Fig. 4: The transient eddy meridional wind variance (color) and the Hoskins/Trenberth flux and its divergence (solid/dashed contour) at 1.0 mbar in a spherical projection during early southern spring (L_s = 190°) from the Mars GCM simulation.

That the transient-eddy activity and hence the requisite heat and momentum fluxes are regionalized can be seen in Fig. 4. This figure shows both the meridional wind variance and the above Hoskings/Trenberth flux (and its divergence) in a spherical projection for fields at about 1.0 mbar. The dominance of the storminess in the western hemisphere and the relatively weak eddy activity in the eastern hemisphere are clearly illuminated. The enhancement of cloud activity in the simulation in

the western hemisphere (not shown) resembles the longitudinal asymmetry indicated in the CRISM observations (Fig. 1) for a mix of CO_2/H_2O ice.

Summary and Future Work: We plan to further investigate the nature of such spatial asymmetries in water vapor and ice-cloud fields during the progression of southern spring to summer, and, to perform correlative studies and diagnostics with large-scale circulation patterns, in order to identify physical mechanisms for such spatial variability.

References:

[1] Banfield, D., et al. (2004) *Icarus*, 170, 365. [2] Hinson D.P. and Wilson, R.J. (2002) *Geophys. Res. Lett.*, 29, 10.1029/2001GL014103. [3] Barnes J.R. (2003) *Mars Atmosphere Modelling and Observations* workshop, Granada, Spain (abstract). [4] Blumsack, S.L., and P.J. Gierasch (1972) *J. Atmos. Sci*., 29, 1081. [5] Pollack, J. B., et al (1981) *J. Atmos. Sci.*, 38, 3. [6] Barnes J.R. et al. (1993) *J. Geophys. Res.*, 98, 3125. [7] Smith, M.D. (2002): *J. Geophys. Res.*, 107, doi: 10.1029/2001JE001522. [8] Smith, M.D. (2004): *Icarus*, 167, 148. [9] Langevin, Y., et al. (2005): *Science*, 307, 1581. [10] Fouchet, F., et al. (2007): *Icarus*, 190, 32. [11] Melchiorri, R., et al. (2007): *Planet. Space Sci*., 55, 333. [12] Langevin, Y., et al. (2007): *J. Geophys. Res.*, 112, 10.1029/2006JE002841. [13] Richardson, M.I., and R.J. Wilson, (2002): *J. Geophys. Res.*, 107, doi: 10.1029/2001JE001536. [14] Richardson, M.I., et al. (2002): *J. Geophys. Res.*, 107, doi: 10.1029/2001-JE001804. [15] Montmessin, F., et al. (2004): *J. Geophys. Res.*, 109, doi: 10.1029/2004JE002284. [16] Brown, A.J., et al. (2007): AGU Fall Meeting, San Francisco, CA (abstract). [17] Seelos, F.P., et al. (2007): LPSC XXXVIII. Houston, TX (abstract). [18] Haberle, R.M., et al. (2008): (this workshop). [20] Hoskins, B.J., et al. (1983) *J. Atmos. Sci.*, 40, 1595. [21] Trenberth, K.E. (1991) *J. Atmos. Sci.*, 48, 2159.

Acknowledgements: This research has been supported by NASA and the Planetary Atmospheres Program within the Planetary Science Division.